American Mineralogist, Volume 73, pages 119–134, 1988

HRTEM characterization of scapolite solid solutions

Ishmael Hassan, Peter R. Buseck
Departments of Geology and Chemistry, Arizona State University, Tempe, Arizona, 85287, U.S.A.

Abstract

The scapolite composition varies between that of the end members marialite $Na_4[Al_3Si_9O_{24}]Cl$ and meionite $Ca_4[Al_6Si_6O_{24}]CO_3$. Two binary solid-solution series exist between the end members: series (a) between 0 and 75% meionite is formed by a coupled replacement $[Na_4 \cdot Cl]Si_2 \rightleftharpoons [NaCa_3 \cdot CO_3]Al_2$, and series (b) between 75 and 100% meionite is formed by a coupled replacement $[NaCa_3 \cdot CO_3]Si \rightleftharpoons [Ca_4 \cdot CO_3]Al$. These reactions behave independently. High-resolution transmission-electron microscopy indicates that series (a) scapolites belong to space group $P4$ or $P4/m$, the result of ordering of the clusters (in the square brackets) and that series (b) scapolites belong to space group $I4/m$, the result of disordered clusters. The ordering of the clusters in series (a) gives rise to antiphase domains; such domains are not observable in series (b). Although crystals from both series may be intergrown, the order-disorder relationships resulting from the net charge differences among the clusters indicate that they give rise to chemical domains, despite the fact that the framework is continuous. The observed compositional variations in scapolite can be explained adequately in terms of the two independent substitution schemes given above. Al–O–Al bonds, which tend to be unfavorable in aluminosilicates, are more numerous in series (b) scapolite; it seems likely that the highly charged $[Ca_4 \cdot CO_3]^{6+}$ clusters stabilize such bonds.

Introduction

Scapolites are a fairly common group of rock-forming aluminosilicate minerals that occur in a wide variety of metamorphic and altered igneous rocks. They are of interest because of their unusual stoichiometry, relative structural complexity, and the possibility that they could act as storage sites for volatiles in the lower crust and upper mantle (Newton and Goldsmith, 1975, 1976; Lovering and White, 1964).

This work forms part of an on-going study to systematize the role of volatile components that are of petrologic importance and that also give rise to important features in framework alumininosilicate mineral groups. These include, for example, the sodalite group (Cl^-, SO_4^{2-}, S^{2-}, OH^-, H_2O; e.g., Hassan et al., 1985), helvite group (S^{2-}; e.g., Hassan and Grundy, 1985), cancrinite group (CO_3^{2-}, SO_4^{2-}, Cl^-, OH^-, H_2O; e.g., Hassan and Grundy, 1984), and scapolite group (Cl^-, CO_3^{2-}, SO_4^{2-}). In all these related mineral groups, large anions are in cages or channels formed by AlO_4 and SiO_4 tetrahedra. Scapolites are interesting minerals to examine with high-resolution transmission-electron microscopy (HRTEM) because they provide an opportunity to study order-disorder among clusters of atoms.

This study indicates that scapolite forms two solid solutions: series (a) between 0 and 75% meionite and series (b) between 75 and 100% meionite. Ordering of $[Na_4 \cdot Cl]^{3+}$ and $[NaCa_3 \cdot CO_3]^{5+}$ clusters occurs in series (a), but the clusters of $[NaCa_3 \cdot CO_3]^{5+}$ and $[Ca_4 \cdot CO_3]^{6+}$ in series (b) are disordered. This difference in ordering arises from the net charge differences among the clusters and provides an adequate explanation for the unusual substitution schemes in scapolite. A preliminary report appeared as an abstract (Hassan and Buseck, 1986).

Previous work

There is no sharp structural change across the scapolite series, so scapolite commonly is considered as a continuous solid-solution series between the end members $Na_4[Al_3Si_9O_{24}]Cl$ (marialite = Ma) and $Ca_4[Al_6Si_6O_{24}]CO_3$ (meionite = Me) (e.g., Deer et al., 1963; Lin, 1975; Lin and Burley, 1973a, 1973b, 1973c, 1975; Levien and Papike, 1976; Strunz, 1978). The meionite percentage [% Me = 100Ca/(Na + Ca)] is used as the chemical index to indicate the compositions of scapolite (Shaw, 1960; Deer et al., 1963). Evans et al. (1969) proposed two substitution schemes for scapolites: between pure Ma and $NaCa_3[Al_5Si_7O_{24}]CO_3$ (Me_{75}), the substitution is $Na_3Si_2Cl \rightleftharpoons Ca_3Al_2CO_3$, and between Me_{75} and Me_{100}, the substitution is NaSi ⇌ CaAl, as in plagioclase feldspars. From Me_{75} to Me_{100}, the anion site is theoretically filled with CO_3^{2-}.

Because of the dual substitution schemes in scapolite, the results of Evans et al. (1969) have been interpreted as indicating two binary solid-solution series that meet at Me_{75} (Ulbrich, 1973a; Oterdoom and Wenk, 1983). Aitken et al. (1984) also suggested the presence of two series because of a change in the space group. However,

0003–004X/88/0102–0119$02.00

previous studies on the compositional variations across the scapolite series, particularly around Me_{75}, show no sharp structural change that would suggest division of the series, so the presence of two binary solid-solution series was still debatable and is addressed in this study.

Lin (1975) suggested that the unusual stoichiometric variations in scapolite arise from the chemical and physical differences between the Cl^- and CO_3^{2-} anions. According to Lin (1975), tilting of the CO_3^{2-} group causes displacement of Ca^{2+} and Na^+ cations along the c axis and ordering of Al^{3+} and Si^{4+} cations. This tilting has not been detected, however, in other structure refinements (Levien and Papike, 1976; Papike and Stephenson, 1966; Aitken et al., 1984). The compositional variations are further explained in terms of local neutralization of electrostatic charges between the tilted CO_3^{2-} groups, the displaced Na and Ca atoms, and the tetrahedral framework cations (Lin, 1975). Chamberlain et al. (1985) interpreted the compositional variations as achieving local charge balance between the Na^+ and Ca^{2+} cations, and Cl^- and CO_3^{2-} anions. They further suggested that the two possible exchange reactions, $NaCl \rightleftharpoons CaCO_3$ and $NaSi \rightleftharpoons CaAl$, do not behave independently.

Based on X-ray diffraction studies, the two established space groups for scapolite are $I4/m$ (Papike and Zoltai, 1965; Papike and Stephenson, 1966; Ulbrich, 1973b; Peterson et al., 1979; Aitken et al., 1984) and $P4_2/n$ (Lin and Burley, 1973a, 1973b, 1973c, 1975; Levien and Papike, 1976). However, based on electron-diffraction studies, the space group is $P4$ or $P4/m$ for intermediate members of the scapolite group (Phakey and Ghose, 1972). This conclusion is supported by Buseck and Iijima (1974) but not by Oterdoom and Wenk (1983).

Scapolite consists of two types of four-membered rings, each of which is made up of AlO_4 and SiO_4 tetrahedra (Fig. 1a). The type 1 ring consists only of T1 tetrahedra that point in the same direction, whereas the type 2 ring consists of both T2 and T3 tetrahedra that point alternately up and down. The two types of rings are connected to form five-membered rings along columns parallel to the c axis (Fig. 1b). Continuous oval-shaped channels contain the Na^+ and Ca^{2+} cations (Fig. 1a). Each Cl^- and CO_3^{2-} anion is surrounded by four (Na,Ca) cations. The resulting anion-cation clusters are in large cages centered at (¼, ¼, ¼) and (¾, ¾, ¾) (Fig. 1b).

The space groups $I4/m$ and $P4_2/n$ reflect almost no difference in the scapolite structure as far as the distribution of the interframework (Ca^{2+}, Na^+, Cl^-, CO_3^{2-}) ions are concerned. The (Na,Ca) atoms are on the same set of equivalent sites (multiplicity 8). The Cl^- and CO_3^{2-} anions also share equivalent sites (multiplicity 2) if the positional disorder of the planar CO_3^{2-} group is ignored and if it is considered as a sphere. However, if the interframework ions in intermediate scapolites were ordered, then neither space group $I4/m$ nor $P4_2/n$ would be adequate for describing their structural roles.

The structural difference between $I4/m$ and $P4_2/n$ for scapolite arises from the Al/Si distribution in the framework. Scapolite in space group $P4_2/n$ contains three tetrahedral sites (T1, T2, T3; Fig. 1), each of multiplicity 8, whereas in space group $I4/m$, T2 and T3 combine (= T2′) to give multiplicity 16. Scapolite contains two formula units per cell, so the composition of $Me_{37.5}$ can be written as $Na_5Ca_3[Al_8Si_{16}O_{48}]Cl \cdot CO_3$. A structure corresponding to this composition, as far as the framework atoms are concerned, is best described by space group $P4_2/n$ (Lin and Burley, 1973a, 1973c; Levien and Papike, 1976). The T1 and T3 sites are fully occupied by Si, and T2 is occupied by Al. This occupancy gives rise to an ordered distribution of Al and Si (Fig. 1) with no Al–O–Al bonds; such bonds tend to be unstable in aluminosilicates (Loewenstein, 1954).

For scapolites that contain more Si than $Me_{37.5}$, the excess Si replaces Al in the T2 site, and the T2 and T3 sites are disordered. In pure Ma, the T2 and T3 sites are equally occupied by ⅝ Si and ⅜ Al (= T2′), and T1 is fully occupied by Si; the symmetry, therefore increases to $I4/m$ (Lin and Burley, 1973a). This disordered arrangement gives rise statistically to $^{45}/_{32}$ Al–O–Al bonds per formula unit in pure Ma (Oterdoom and Wenk, 1983).

For scapolites that contain more Al than in $Me_{37.5}$, it appears that neither the T2 nor T3 site can contain more than 0.50 Al and that therefore Al replaces Si in the T1 sites. The T2 and T3 sites also attain a disordered Al-Si distribution so as to reduce the number of Al–O–Al bonds formed (Lin and Burley, 1973a). In pure Me, each of the three tetrahedral sites contains ½ Si + ½ Al, and the symmetry therefore increases to $I4/m$. This disordering gives rise statistically to ⅔ Al–O–Al bonds per formula unit in pure Me (Oterdoom and Wenk, 1983). Klee (1974a, 1974b) has shown that it is theoretically possible to avoid Al–O–Al bonds up to an Al/Si ratio of 5/7 (i.e., Me_{75}) by having 50% Al on T1 and 37.5% Al on T2 (= T3).

The Al–O–Al avoidance rule holds in framework aluminosilicates that have an Al/Si ratio of 1:1, as in anorthite, sodalite-group, and cancrinite-group minerals. Al and Si are presumably also distributed in a fully ordered manner in pure Me, which also has an Al:Si ratio of 1:1. The problem is that scapolite contains five-membered rings. In pure Me, one-half of these rings must contain 3 Al and 2 Si tetrahedra, so the Al–O–Al avoidance rule has to be broken.

Lin and Burley (1973c) have shown that the intensities of the type b ($h + k + l$ = odd) reflections are strongest for $Me_{37.5}$ and decrease (extrapolated) to zero at the end members Ma and Me (Fig. 2). They attribute these changes to Al-Si ordering on the T2 and T3 sites. In $Me_{37.5}$, the $Cl:CO_3$ ratio is 1:1, and they suggested that distortions arising from substitutions of these anions add to the intensities of the type b reflections. Antiphase domains are observable only with type b reflections. These domains are interpreted as arising from either ordering of Cl^- and CO_3^{2-} (Phakey and Ghose, 1972) or from Al-Si ordering in samples that contain little Cl^- (Oterdoom and Wenk, 1983).

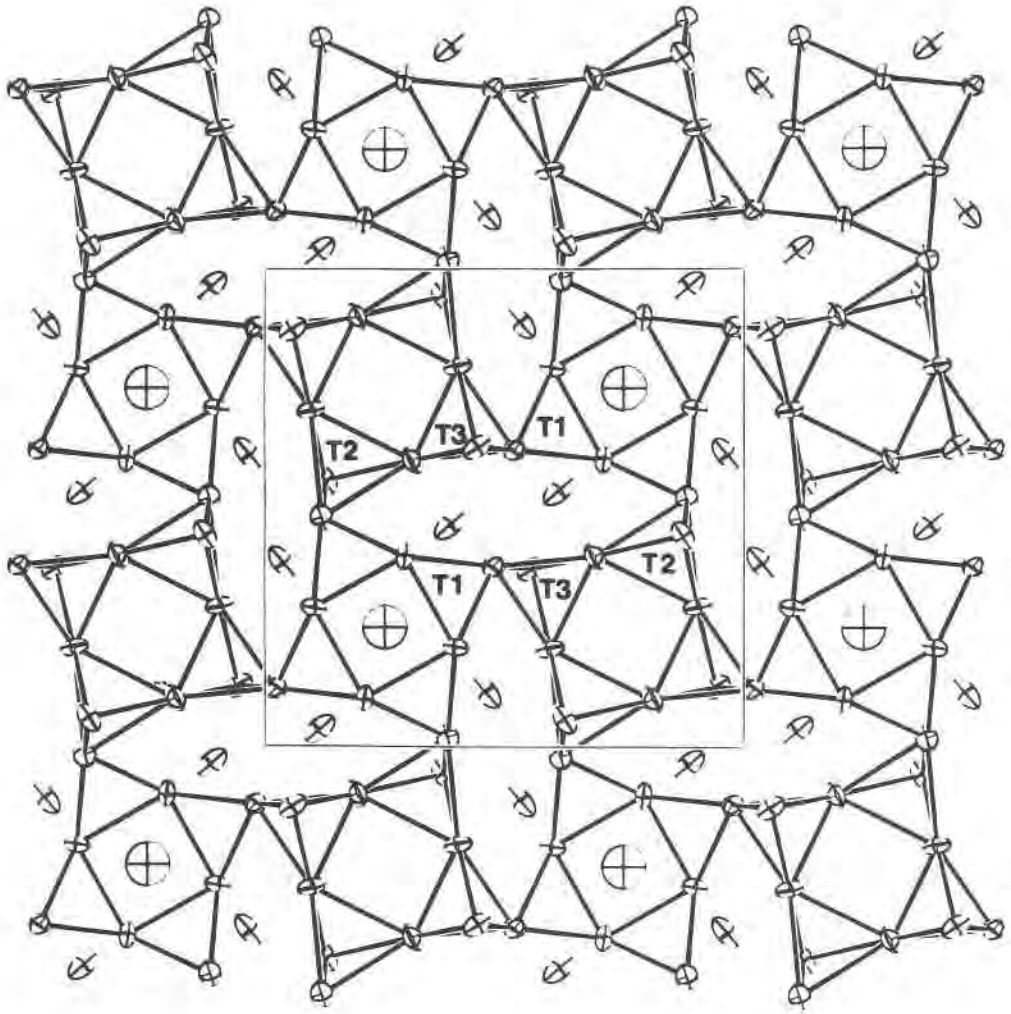

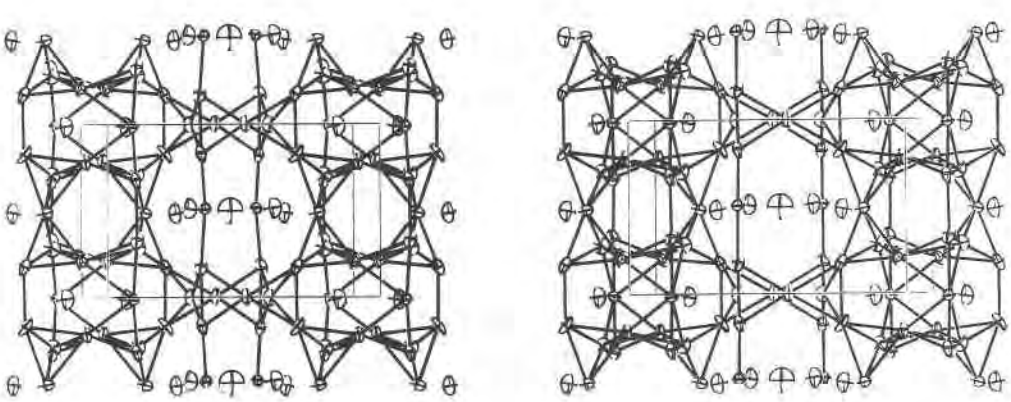

Fig. 1. The structure of marialite scapolite, with the unit cell outlined. The framework tetrahedral sites are labeled. The Cl atoms are drawn largest, followed by Na, then oxygen atoms. (a) Projection along *c* axis showing the two types of four-membered rings and the continuous, oval-shaped channels that contain the Na atoms. (b) Stereoscopic *b*-axis projection (*c*-axis vertical) showing a large cage that contains $[Na_4 \cdot Cl]^{3+}$ types of clusters and columns that contain the five-membered rings in which Al–O–Al bonds can be formed. Data from Levien and Papike (1976) and drawn using ORTEP (Stewart, 1976).

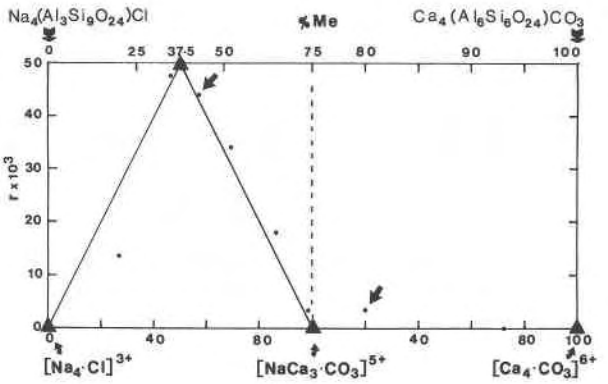

Fig. 2. The relationship between the intensity ratio r of type b to type a reflections ($r = \Sigma I(h + k + l = \text{odd})/\Sigma I(h + k + l = \text{even})$ and percent Me, and also r versus end-member cluster percentage derived from percent Me. The dashed line shows the division of the compositional series at Me_{75}. Note that from Me_{75}, there is a change in scale on the percent Me axis. However, the scale on the cluster-axis is linear. In each series, the scale is given in terms of percentage of the end-member cluster that is on the right. The largest r value occurs in the $Me_{37.5}$ scapolite, where the $[Na_4 \cdot Cl]^{3+} : [NaCa_3 \cdot CO_3]^{5+}$ ratio is 1:1. If the clusters are disordered, the r value should be zero in pure Ma and also in Me_{75} to Me_{100}. The solid triangles represent theoretical data points. The experimental data points (solid dots) are from Lin and Burley (1973c), and their variation was represented by a curve. Solid lines serve as reference to indicate the deviation of the data from linearity. The two samples used in this study are indicated by straight arrows.

Electrostatic energy calculations for $Me_{37.5}$ indicate that the energy is minimized if Na^+ is adjacent to Cl^- and if Ca^{2+} is adjacent to CO_3^{2-} (Chamberlain et al., 1985). Moreover, these calculations suggest that short-range ordering of $[Na_4 \cdot Cl]^{3+}$ and $[Ca_4 \cdot CO_3]^{6+}$ clusters is energetically favorable and might give rise to antiphase domains.

Scapolite structural models

According to the X-ray structures of scapolite, the two cages per cell are identical as far as the Al-Si framework is concerned. In the end members Ma and Me, the cages contain $[Na_4 \cdot Cl]^{3+}$ and $[Ca_4 \cdot CO_3]^{6+}$ clusters, respectively. If these clusters were the only types in the intermediate members, then for any ratio of these clusters, we should get a valid composition for scapolite. For example, a ratio of $[Na_4 \cdot Cl]^{3+}$ to $[Ca_4 \cdot CO_3]^{6+}$ of 1:1 implies that in Me_{50} the $Cl:CO_3$ ratio is 1:1. However, this ratio occurs in $Me_{37.5}$. Thus, the occurrence of only $[Na_4 \cdot Cl]^{3+}$ and $[Ca_4 \cdot CO_3]^{6+}$ clusters cannot give rise to the observed compositional variations in scapolite. The additional occurrence of at least $[NaCa_3 \cdot CO_3]^{5+}$ clusters is necessary to explain scapolite compositional variations, as is shown in this study. The electrostatic energy calculations are based on $Me_{37.5}$, so the calculations also indicate that ordering of $[Na_4 \cdot Cl]^{3+}$ and $[NaCa_3 \cdot CO_3]^{5+}$ clusters is energetically favorable (Chamberlain et al., 1985).

The coupled substitution in series (a) may be written as $[Na_4 \cdot Cl]Si_2 \rightleftharpoons [NaCa_3 \cdot CO_3]Al_2$. In series (a), the clusters are expected to order because of the overall charge difference of +2 valence units (v.u.) (+3 v.u. for $[Na_4 \cdot Cl]^{3+}$ clusters and +5 v.u. for $[NaCa_3 \cdot CO_3]^{5+}$ clusters). Such cluster ordering may also be coupled to Al-Si ordering. In series (b), the coupled substitution is $[NaCa_3 \cdot CO_3]Si \rightleftharpoons [Ca_4 \cdot CO_3]Al$; however, because of the net charge difference of +1 v.u. between the clusters there is less tendency for them to order. In series (b), we consider ordering of Na^+ and Ca^{2+} cations since both anion sites are filled with CO_3^{2-}, and the compositional difference between the clusters can be expressed as a $Na^+ \rightleftharpoons Ca^{2+}$ substitution. These two cations have similar radii and commonly substitute for each other, so Na-Ca disordering may be expected.

Al and Si ordering is possible across the scapolite series; however, HRTEM cannot distinguish Al^{3+} from Si^{4+} because of their similar scattering powers. This type of ordering is currently being studied by the MAS NMR technique, and preliminary results were reported by Sherriff et al. (1986).

Materials used

Samples from the study of Evans et al. (1969) were made available to us by D. M. Shaw. We chose a crystal with composition $Me_{39.5}$ (sample 0N70 in Evans et al., 1969) because its composition is close to the $Me_{37.5}$ composition that shows the strongest type b reflections (Fig. 2). The sample is from Mpwapwa, Tanzania, where it occurs in quartzofeldspathic gneiss. The crystals are transparent pale-yellow and of gem quality. The second sample has composition $Me_{79.6}$ (sample 0N47 in Evans et al., 1969) from Slyudyanka, Siberia, USSR and is of unknown occurrence. The crystals are white, brittle, and bladed. Of the samples that were available to us, this sample is closest in composition to the Me end member.

Electron microscopy

Electron microscopy was performed using a JEOL 200CX electron microscope operated at 200 keV with a LaB_6 filament. A ±12° double-tilt, top-entry goniometer stage was used. The spherical aberration coefficient, C_s, of the objective lens was 1.2 mm. A 40-μm (i.e., radius of 0.76 $Å^{-1}$) objective aperture was centered about the incident beam, and a 400-μm condenser aperture was used to record images at 530 000 magnification.

Fragments of scapolite suitable for study were obtained by crushing the mineral in acetone using an agate mortar and pestle. The crystals in suspension were deposited on holey carbon support films, and HRTEM data were recorded from thin regions.

Image simulations

Prior to the present study it was unclear whether it would be possible to distinguish clusters of $[Na_4 \cdot Cl]^{3+}$ from $[NaCa_3 \cdot CO_3]^{5+}$ using HRTEM imaging. Owing to the instability of scapolite in the electron beam (Buseck and Iijima, 1974), it was decided to by-pass the painstaking task of working with such materials until we were convinced by image simulations that the different clusters could be distinguished from each other.

*S*imulations of *h*igh-*r*esolution *l*attice *i*mages were ob-

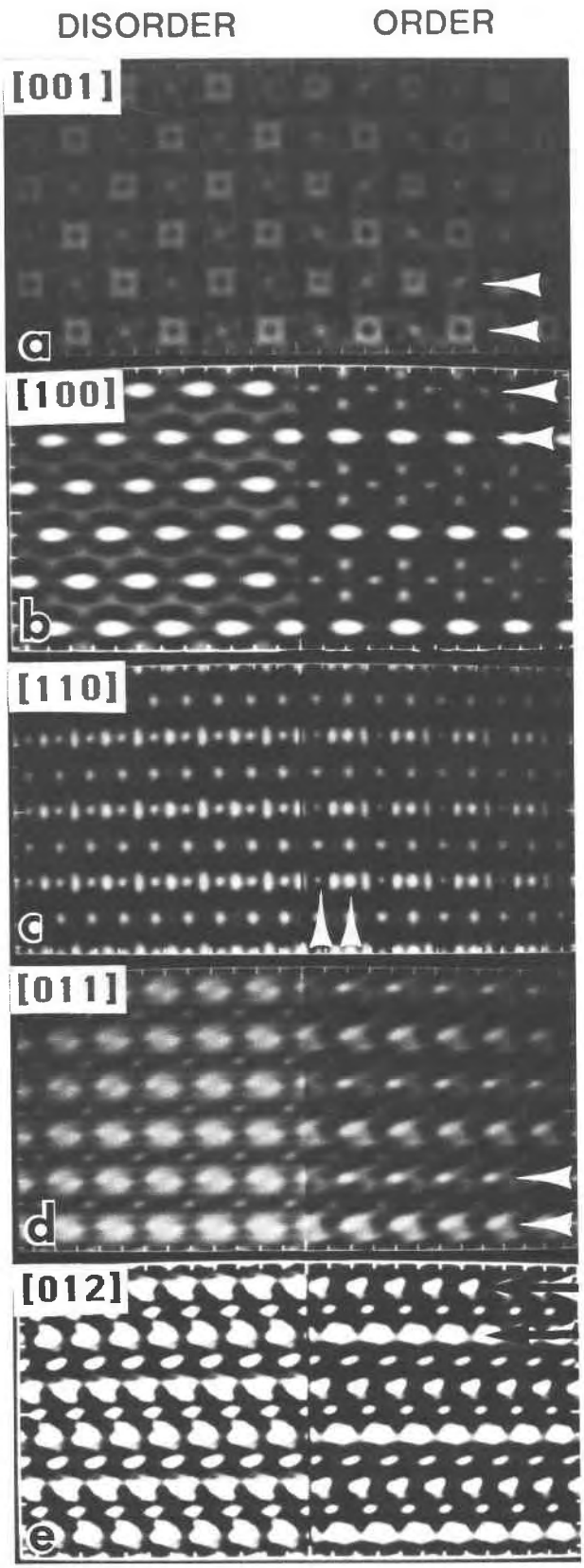

tained with the SHRLI set of programs (O'Keefe and Buseck, 1979; O'Keefe et al., 1978), which are based on the multislice method (Goodman and Moodie, 1974; Cowley and Moodie, 1957). Images were calculated for several projection directions over a range of defocus (Δf) from -400 to -1400 Å (increments of 100 Å) and for crystal thicknesses (H) from about 3 to 200 Å (increments corresponding to the repeat distance in the projection direction). Calculations were performed using the electron optical parameters given above for the JEOL 200CX microscope, together with a divergence angle of 0.001 radian (estimated from the width of a diffraction spot under imaging conditions) and a depth of focus of 50 Å.

Image simulations were made for two structural models based on the $Me_{37.5}$ composition (with tetragonal cell parameters $a = b = 12.069$ Å and $c = 7.581$ Å). A disordered model is based on the average X-ray structure ($P4_2/n$) of Levien and Papike (1976), and an ordered model is based on the same framework, but with the clusters $[Na_4 \cdot Cl]^{3+}$ and $[Ca_3Na \cdot CO_3]^{5+}$ ordered in the cages at (¼, ¼, ¼) and (¾, ¾, ¾), respectively. These structural models were input in space group $P1$ for the purpose of image calculations. The simulated images were all output on the same relative contrast scale.

Through-thickness, through-focus series of images for all the projections show systematic trends. Although the images are nearly thickness independent for the range calculated, the objective-lens defocus is critical. Figure 3 shows a comparison of a set of calculated images for various zone axes in the two structural models. These images are selected because they provide the maximum contrast differences. Differences between the two structural models are seen in all the projections of Figure 3, but with varied degrees of clarity. The arrows mark rows that are identical in the disordered model but that differ in the ordered model. For example, the [001] zone shows the positions of the clusters as having the same contrast for the disordered model and different contrast for the ordered model. In the [001] zone, the clusters correspond to the positions of the large white spots with dark centers. $[Na_4 \cdot Cl]^{3+}$ is lighter and $[NaCa_3 \cdot CO_3]^{5+}$ is darker, but the difference is not great. This small difference would be difficult to detect in experimental images. Similar small differences also occur for the [110] zone. However, the calculated images for zones [100], [011], and [012] clearly show differences between the two models that could allow them to be distinguished from each other in experimental images.

The images are strongly defocus dependent, so the two models are only distinguishable at specific defocus values; these values change with thickness and projection direc-

←

Fig. 3. Calculated images for ordered and disordered structural models. In the following zones, the values for thickness (Å) and defocus (Å), respectively, are (a) [001]: 22.7, −800; (b) [100]: 72.4, −1200; (c) [110]: 76.8, −800; (d) [011]: 51.4, −800; (e) [012]: 75.9, −1200.

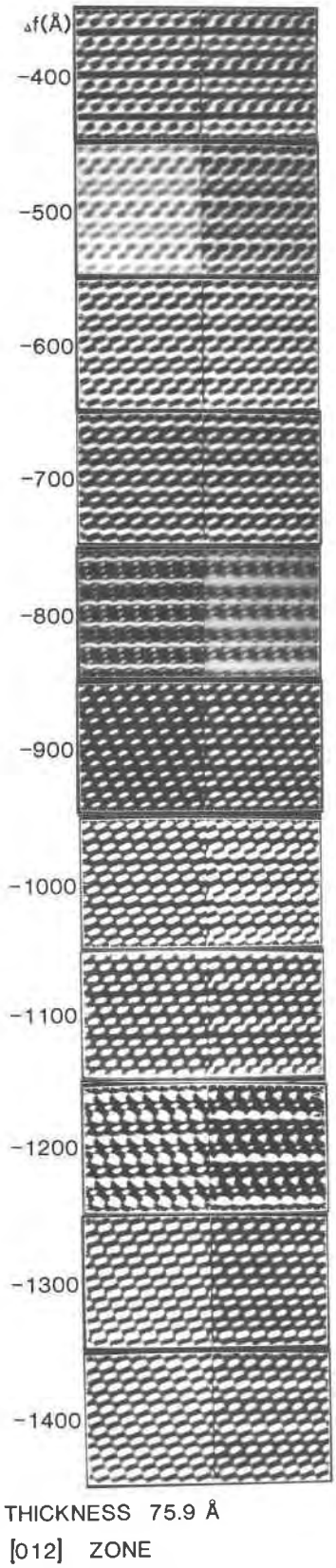

Fig. 4. Comparison of defocus effect for a 75.9-Å thickness in the [012] zone for the ordered (right) and disordered (left) models.

tion. This point is illustrated in Figure 4 for the projection along the [012] zone for the two structural models. The calculated images show that the two models are only clearly distinguishable at the defocus value of −1200 Å. Similar features occur for the other projections. Therefore, extreme care is necessary in recording and interpreting the experimental images; otherwise the results could be misleading.

Electron-diffraction patterns

Reciprocal-space observations of scapolite show that the reflections can be divided into four types:

1. Type a: $(h + k + l)$ = even. These occur as strong diffraction maxima.

2. Type b: $(h + k + l)$ = odd. These occur as sharp spots and are weaker than type a reflections. They are forbidden in space group $I4/m$.

3. Type c: $(00l)$, l = odd. Although forbidden in both space groups $I4/m$ and $P4_2/n$, they appear as sharp spots in some scapolite diffraction patterns. They violate the existence of the 4_2 screw axis in space group $P4_2/n$.

4. Type d: $(hk0)$, $h + k$ = odd. Although forbidden in both space groups $I4/m$ and $P4_2/n$, they are present as sharp spots in some scapolite diffraction patterns. They violate the existence of the n glide plane in space group $P4_2/n$.

The type c and type d reflections do not disappear on tilting about systematic rows containing these spots, and therefore they are unlikely to be caused by multiple diffraction. Moreover, they were recorded both at 200 keV and with a Phillips 400T microscope operating at 100 keV, and they show no difference.

A [001]-zone *s*elected *a*rea *e*lectron *d*iffraction (SAED) pattern for $Me_{39\,5}$ is shown in Figure 5a. Similar patterns were obtained for the $Me_{79\,6}$. In over-exposed SAED patterns for the [001] zone (not shown), type d reflections occur as diffuse spots in the zero-order Laue zone, and sharp but weak type b reflections occur in the first-order Laue zone. These reflections, however, appear stronger in other zones (Fig. 5b). Moreover, the ordering reflections cannot occur by multiple diffraction in the [001] zone.

The $Me_{39\,5}$ crystals (Figs. 6a, 6d) and some of the $Me_{79\,6}$ crystals (Figs. 6b, 6e) have similar reflections. These SAED patterns show reflections of types b, c, and d that are absent for some of the $Me_{79\,6}$ crystals (Figs. 6c, 6f), indicating that there is local variation in composition or ordering within the $Me_{79\,6}$ sample.

Reflections of types b and c for the [100] zone are weak compared to type a reflections. However, in the [011] zone, type b and type d reflections are strong compared to the type a reflections, and they do not decrease in intensity as rapidly with beam exposure as they do in the [100] zone. Therefore, different results may be obtained for different orientations, depending on the time taken to record the images because scapolite damages more in some orientations than in others. The reflections of types b, c, and d can be made to disappear without losing all of the

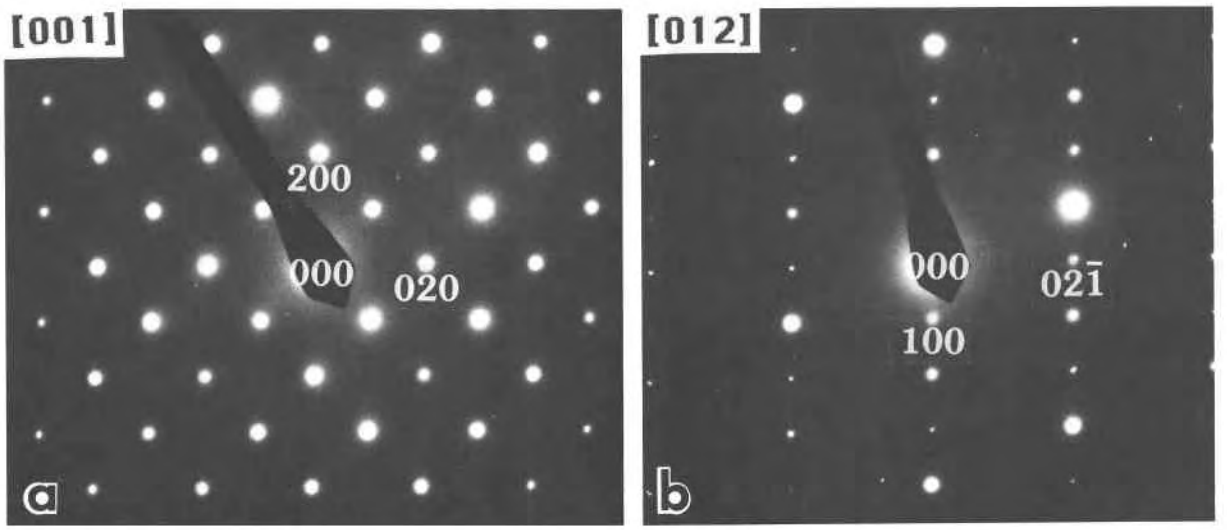

Fig. 5. (a) A [001]-zone SAED pattern showing type a reflections. (b) A [012]-zone SAED pattern for the $Me_{39.5}$ sample showing strong type b (e.g., 02$\bar{1}$, $\bar{1}4\bar{2}$, 22$\bar{1}$, 14$\bar{2}$) and type d (e.g., 100, 300, 500) reflections.

intensities in the main type a reflections. This effect is particularly evident for the [001] and [100] zones. Levien and Papike (1976) observed that the reflections that violate $I4/m$ symmetry decrease considerably in intensity with temperature up to 1000 °C but do not disappear. Throughout this temperature range, the constancy of the Al–O and Si–O bonds indicate practically no Al-Si disorder. These observations, therefore, suggest that Al-Si order cannot solely be related to the reflections that violate $I4/m$ symmetry. Moreover, beam-damage and heating seem to cause disordering of the interframework ions.

The electron-diffraction results suggest that either $P4$ or $P4/m$ is the likely space group for intermediate scapolites that contain Cl^-. Crystals that tend to be Cl free only show type a reflections (some crystal fragments from $Me_{79.6}$, this study; Me_{77}, Peterson et al., 1979; synthetic Me_{84}, Aitken et al., 1984; Me_{93}, Lin and Burley, 1973c; Ulbrich, 1973b). Published chemical analyses for these samples also indicate that they contain little or no Cl^-. The Cl-free crystals and the end member Ma, therefore, belong to space group $I4/m$.

High-resolution images of scapolite

In order to estimate the effect of beam-damage, we routinely recorded SAED patterns before and after imaging. Optical diffractograms were made from the experimental images to determine which reflections contributed to the images. All suitable images were matched by detailed image simulations.

In all the images given below, structure projections are scaled and oriented so that they superimpose directly on the electron micrographs. Their positioning is based on comparison between the simulated and experimental images. In the structure projections, the $[Na_4 \cdot Cl]^{3+}$ clusters are unshaded and $[NaCa_3 \cdot CO_3]^{5+}$ clusters are shaded to indicate cluster ordering. The framework atoms are shown as small dots with the size of the tetrahedral cations being smaller. The unit cells in the structure projections serve as scales.

The [001] SAED pattern shows only type a reflections in this orientation (Fig. 5a), and therefore ordering of clusters cannot be seen in the [001] image (not shown). A [001] image was shown by Buseck and Iijima (1974), and some images are given below but discussed in a different context (Fig. 11).

The SAED pattern for the [100] zone (Fig. 6a) shows that the extra reflections are weak compared to the main type a reflections. An optical diffractogram of a [100] image does not show the 001 and 010 reflections, but it shows weak 021 reflections; however, the indicated ordering is not evident in the image (not shown).

The SAED pattern for the [012] zone (insert in Fig. 7) was photographed before and after imaging and did not change significantly, thus indicating little beam damage to the crystal. An optical diffractogram of the image (insert in Fig. 7) shows that the crystal is well oriented and, in particular, that the 001 and 02$\bar{1}$ reflections (arrows) are present. The experimental image (Fig. 7) shows contrast that arises from ordering of $[Na_4 \cdot Cl]^{3+}$ and $[NaCa_3 \cdot CO_3]^{5+}$ clusters. These contrast differences are seen along alternating planes {02$\bar{1}$} and {04$\bar{2}$} (long arrows), and {100} and {200} (short arrows).

The experimental and the calculated images (Fig. 7) suggest that the Na^+ and the Ca^{2+} positions, while difficult to see, are distinguishable. The Ca^{2+} positions appear darker on both sides of the dark rows of spots, whereas the Na^+ positions appear lighter on both sides of the white rows of spots.

The contrast of equivalent spots varies considerably across the experimental image (Fig. 7) and is even more pronounced in some images for the $Me_{79.6}$ sample (not shown). Although this effect may arise from beam dam-

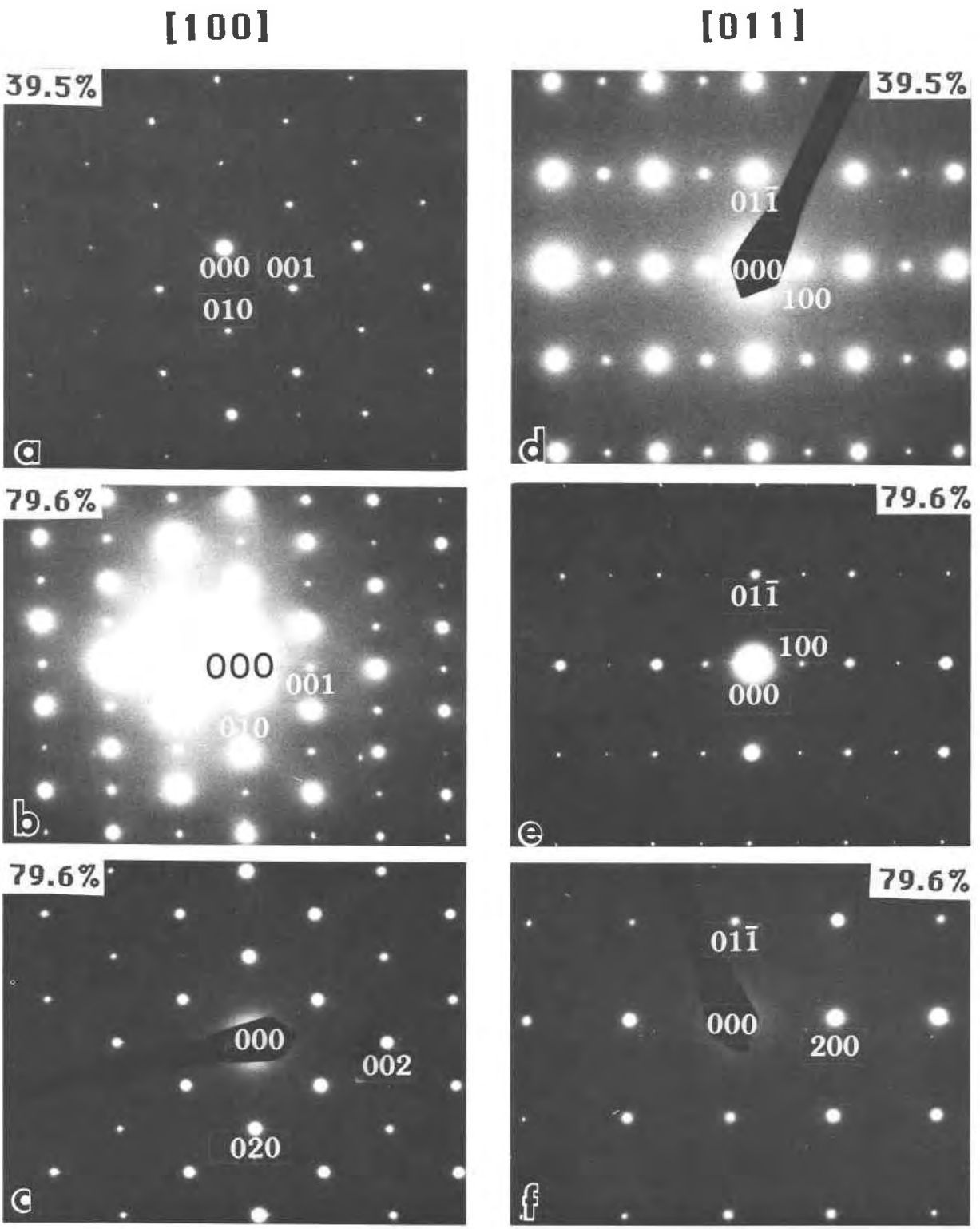

Fig. 6. Comparison of [100] (Figs. 6a, 6b, 6c) and [011] (Figs. 6d, 6e, 6f) SAED patterns for $Me_{39.5}$ (Figs. 6a, 6d) and $Me_{79.6}$ (Figs. 6b, 6c, 6e, 6f). Reflections of the following types are shown: type b (Figs. 6a, 6b contain 021, 012, 014, 032, etc.; Figs. 6d, 6e contain $11\bar{1}$, $12\bar{2}$, etc), type c (Figs. 6a, 6d contain 001, 003, etc.), and type d (Figs. 6d, 6e contain 100, 300, etc.). These reflections are absent in some crystal fragments of the $Me_{79.6}$ sample (Figs. 6c, 6f).

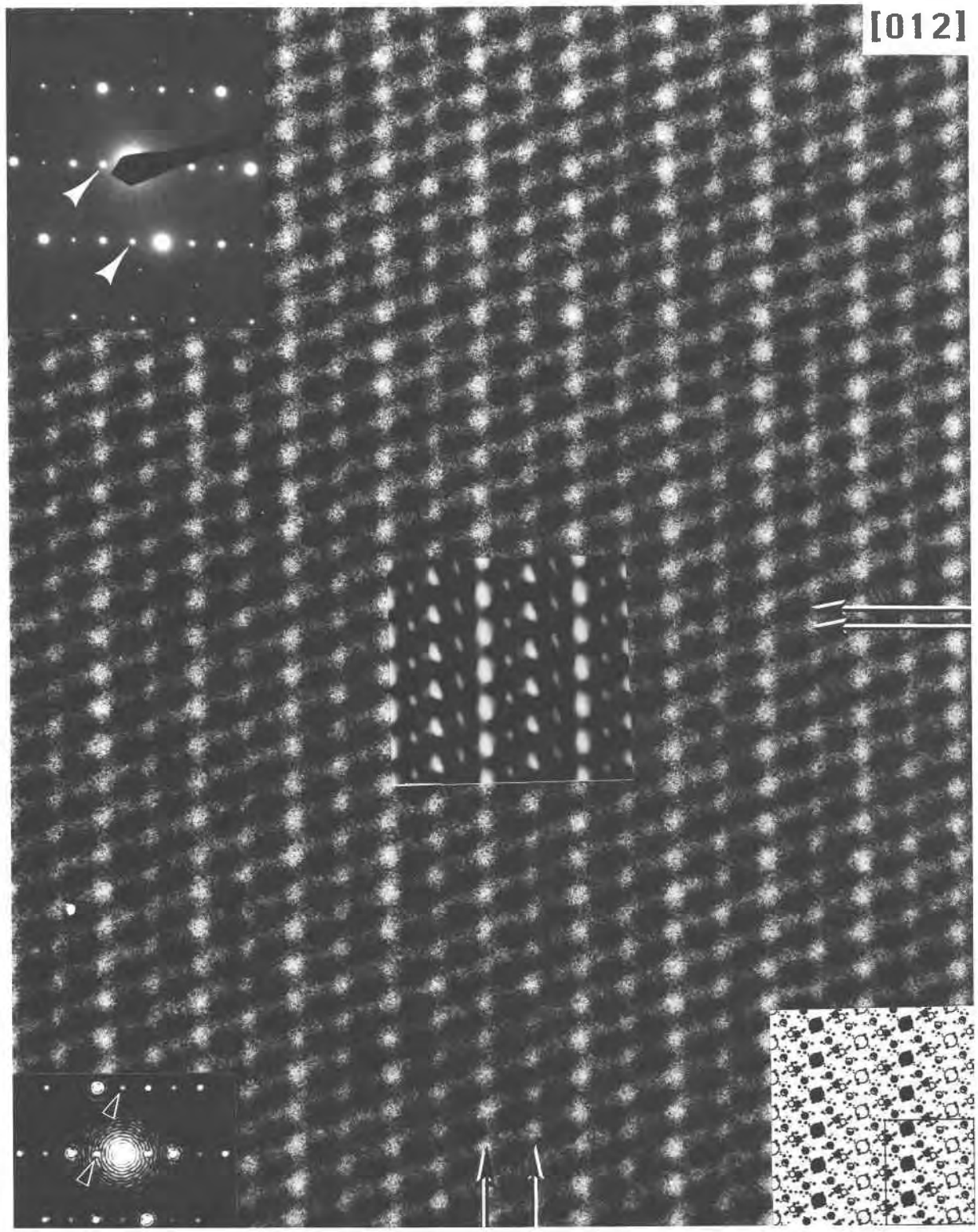

Fig. 7. A [012] image of the $Me_{39.5}$ sample. The SAED pattern and the optical diffractogram are shown as inserts at the upper- and lower-left, respectively. The simulated image in the central insert is based on the ordered model (H = 75.9 Å, $\Delta f = -1200$ Å; cf. Fig. 3e). The projected structure (lower right; the a axis is horizontal and the [02$\bar{1}$] axis is vertical) shows ordering of $[NaCa_3 \cdot CO_3]^{5+}$ and $[Na_4 \cdot Cl]^{3+}$ clusters that is evident in the image.

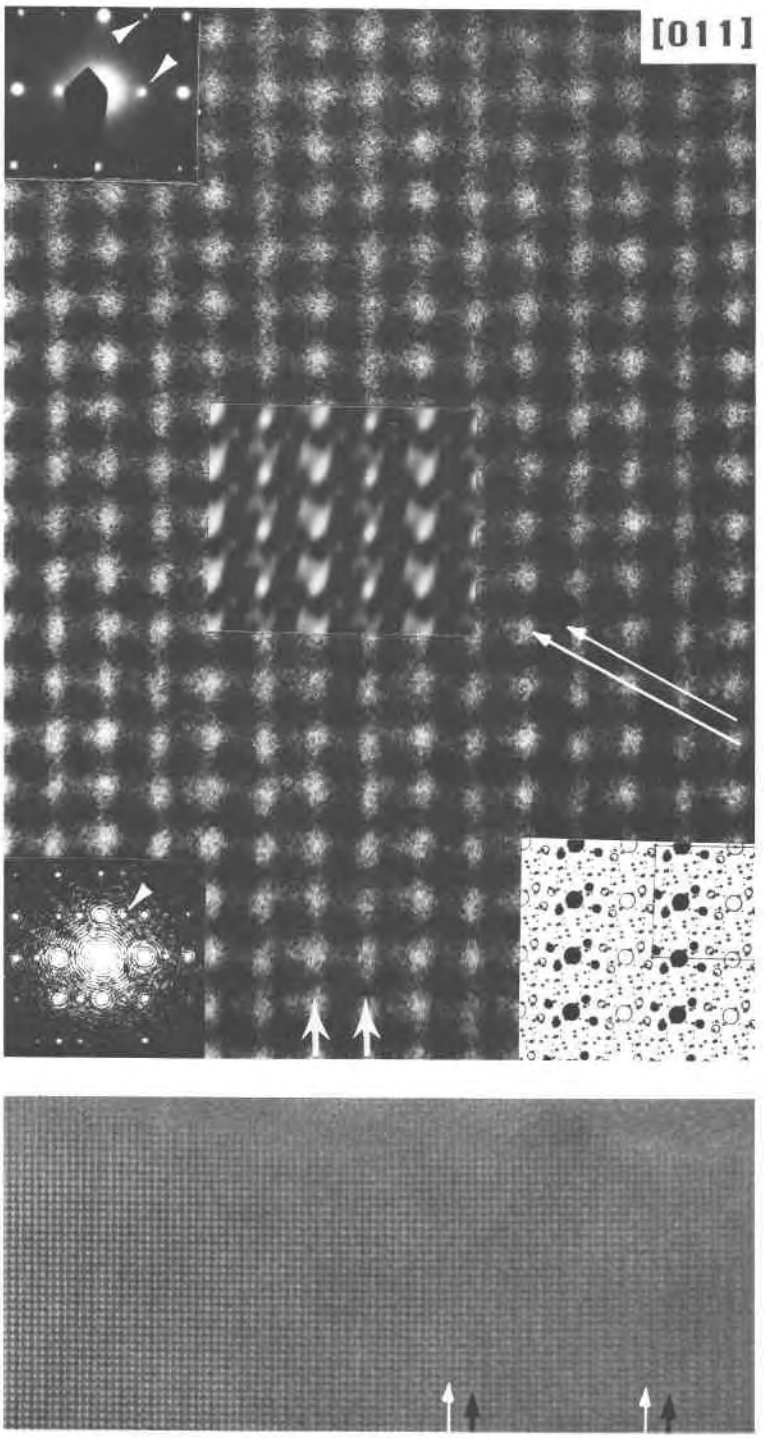

Fig. 8. A [011] HRTEM image (top) and low-magnification image (bottom) of the $Me_{39.5}$ sample. Inserts of the SAED pattern and optical diffractogram are given in the upper- and lower-left corners, respectively, in the image at the top. The calculated image in the central insert is based on the ordered model (H = 51.4 Å, $\Delta f = -800$ Å; cf. Fig. 3d). Ordering of $[Na_4 \cdot Cl]^{3+}$ and $[NaCa_3 \cdot CO_3]^{5+}$ clusters is indicated in the projected structure (lower-right corner; the a axis is horizontal and [011] is vertical) and is more evident in the image shown at the bottom in which white and black arrows point out rows that have light and dark contrast, respectively.

age, it is interpreted as disorder, reflecting the excess amount of one cluster over the other since their ratio is not 1:1 in the sample. Moreover, this randomness of equivalent spots showing different contrasts cannot give rise to the sharp spots seen on the SAED patterns.

The calculated [012] image based on the disordered model (Fig. 3e) does not match the experimental image (Fig. 7) nearly as well as the calculated image for the ordered model. Nevertheless, calculated images based on the disordered model were simulated with both crystal tilt and beam tilt introduced as variables, as these variables can give rise to image artifacts (Smith et al., 1983). However, it was not possible to reproduce the experimental image (Fig. 7) by using the disordered model and

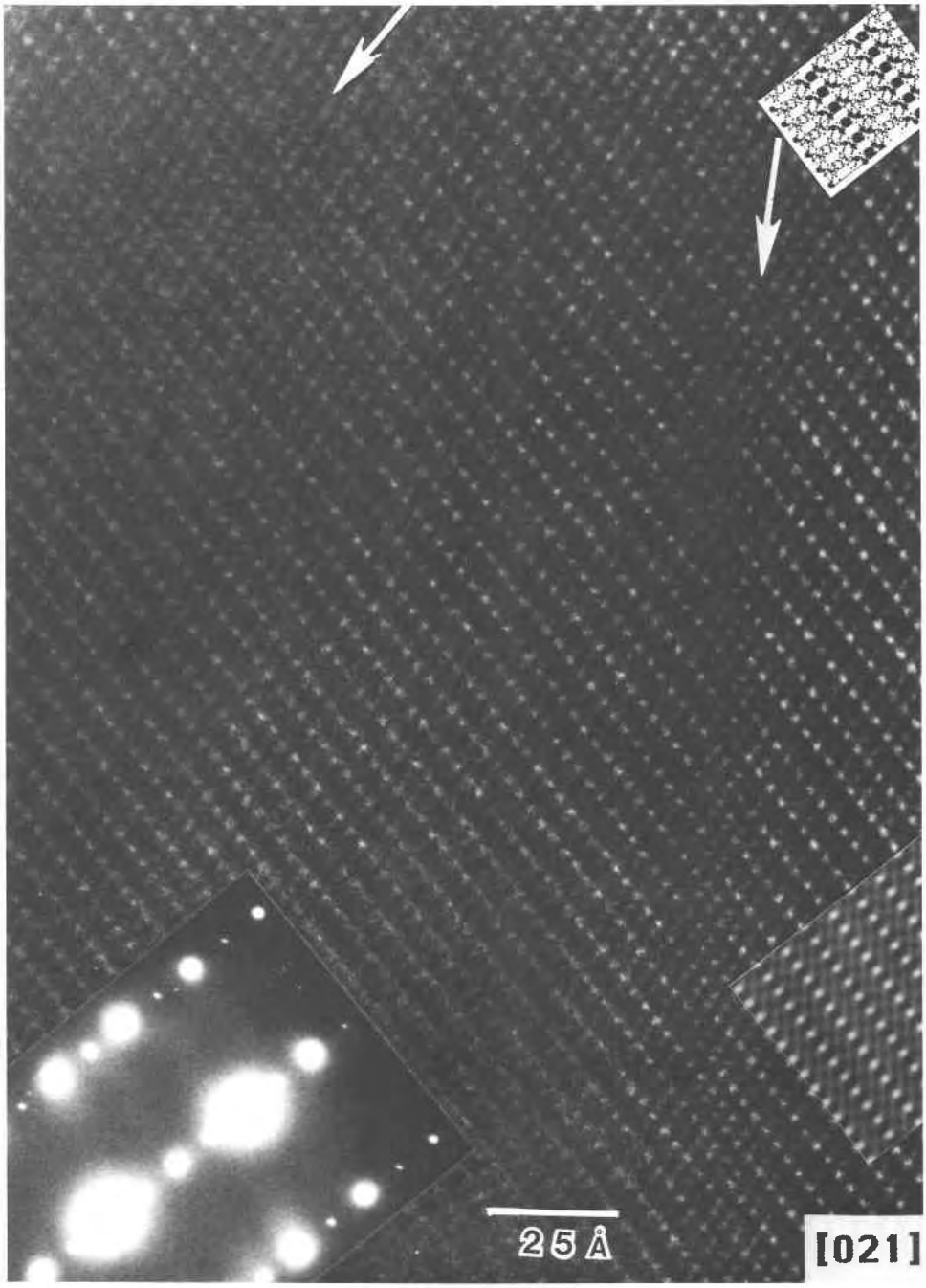

Fig. 9. A [021] image of the $Me_{39.5}$ sample showing a sharp APB (arrows).

these additional variables. Therefore, we conclude that the observed variation in contrast in Figure 7 arises from ordering of $[Na_4 \cdot Cl]^{3+}$ and $[NaCa_3 \cdot CO_3]^{5+}$ clusters and not from experimental variables. The ordering of these clusters is also shown in Figure 8. The SAED pattern and optical diffractogram (inserts in Fig. 8) show the $11\bar{1}$ and 100 reflections (arrows); alternating $\{11\bar{1}\}$ and $\{22\bar{2}\}$ planes (long arrows) and $\{100\}$ and $\{200\}$ planes (short arrows) show different contrast in the image. This ordering may be easier to see in the low-magnification image shown at the bottom of Figure 8, where it is separated from the HRTEM image at the top.

Antiphase domains in scapolite

The observed ordering of $[Na_4 \cdot Cl]^{3+}$ and $[NaCa_3 \cdot CO_3]^{5+}$ clusters can give rise to antiphase domains. If the cavity at (¼, ¼, ¼) is occupied by $[Na_4 \cdot Cl]^{3+}$ clusters, then the (¾, ¾, ¾) cavity would be occupied by $[NaCa_3 \cdot CO_3]^{5+}$

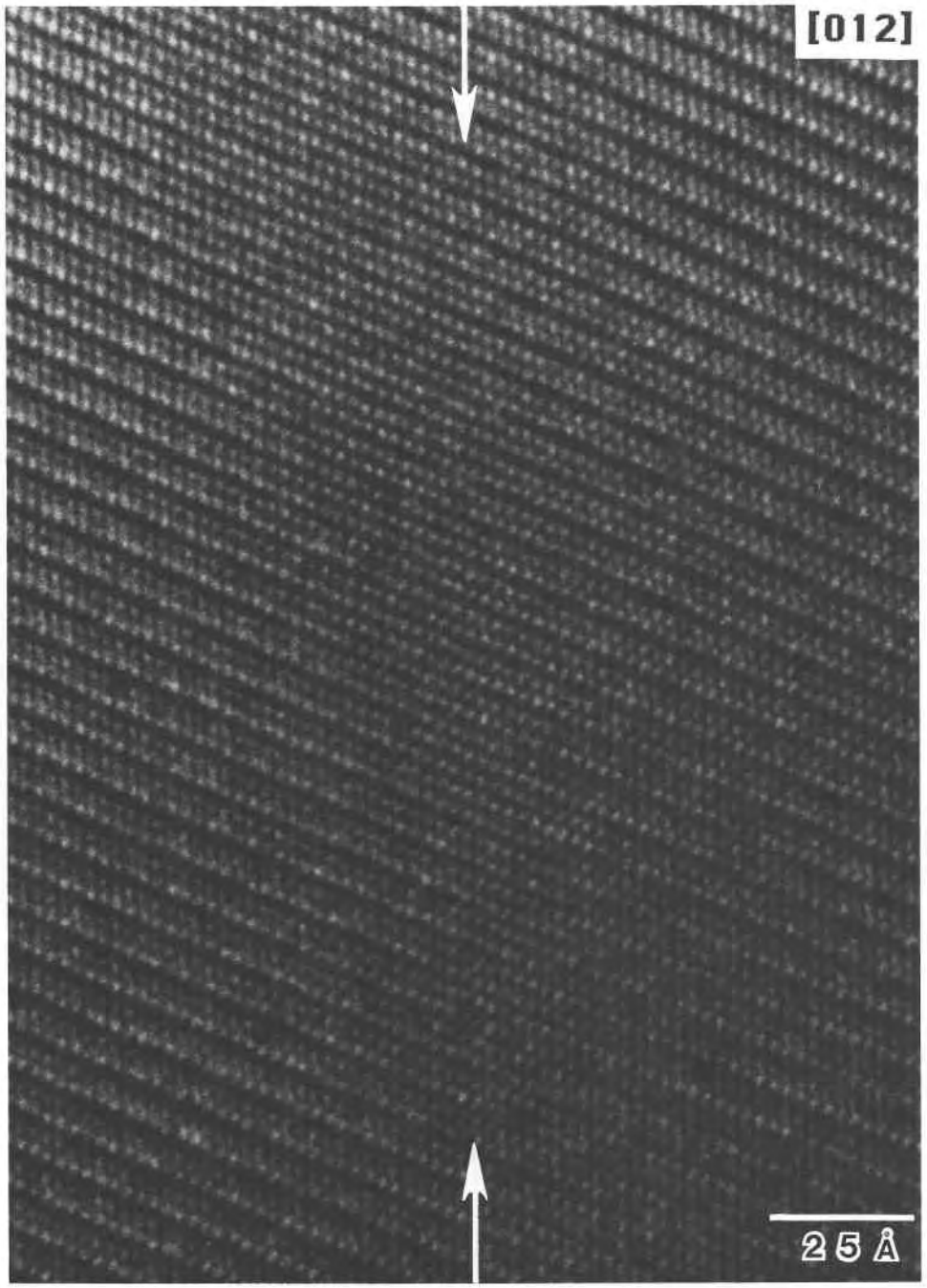

Fig. 10. A [012] image of the $Me_{39.5}$ sample showing a wide APB (arrows).

clusters; in the adjacent domain the occupancy of the cavities could be reversed. Antiphase domain boundaries (APBs) in scapolite are difficult to image in HRTEM mode; they cannot be seen on the TEM screen but only on photographic prints.

Figure 9 shows an APB having the shape of a question mark. The fringes are shifted by $\frac{1}{2}a_0$ across the sharp APB (arrows). The projected structure, the simulated image, and the SAED pattern are also shown as inserts in Figure 9. Figure 10 shows a wider APB (arrows). A SAED pattern, simulated images, and a HRTEM image for this projection are given in Figures 5b, 3e and 4, and 7, respectively. Shifts in fringes can also arise from a change in thickness, but simulated images for thicknesses up to 165.2 Å ([021] zone) and 177.2 Å ([012] zone), respectively, do not show any shift or reversal of contrast of the

lattice fringes. We interpret these APBs as arising from ordering of $[Na_4 \cdot CL]^{3+}$ and $[NaCa_3 \cdot CO_3]^{5+}$ clusters in scapolite.

Chemical domains in the $Me_{79.6}$ scapolite

The electron-diffraction results, particularly Figure 6, suggest that there is local variation in composition or ordering within the $Me_{79.6}$ sample and that Cl-free scapolites generally show only type a reflections. Moreover, the HRTEM images show ordering of $[Na_4 \cdot Cl]^{3+}$ and $[NaCa_3 \cdot CO_3]^{5+}$ clusters in series (a) scapolite ($Me_{39.5}$ and some crystals of $Me_{79.6}$) and lack of ordering of $[NaCa_3 \cdot CO_3]^{5+}$ and $[Ca_4 \cdot CO_3]^{6+}$ clusters in series (b) scapolite (some crystals of $Me_{79.6}$).

Figures 11a, 11b, and 11c were taken at about 15-s intervals from one region of a $Me_{79.6}$ crystal. This series of exposures shows the results of reactions that are caused by the electron beam. The images show a continuous crystal that is made up largely of series (b), with inclusions of many smaller domains that are presumably Cl-bearing from series (a). If these figures are viewed at low angle along the direction of the large arrow [i.e., along the (110) planes], it can be seen that the (110) planes are shifted by ½(110) in the many small (Cl-rich?) domains in Figures 11a and 11b, but not in Figure 11c. This shift in fringes occurs in a direction associated with type a reflections and cannot arise from APBs.

Optical diffractograms were taken from all images in Figure 11, and they show only type a reflections with minor change in intensities from one image to another. This observation does not rule out the possibility of ordering of clusters in the many small (Cl-rich?) domains because they may be too small to give additional reflections.

The sizes of the (Cl-rich?) domains decrease from Figure 11a to 11b, until in Figure 11c the entire crystal appears homogeneous. These observations indicate that the electron beam induces disordering among all the clusters. More importantly, the results suggest that crystals from series (a) and (b) form chemical domains because the two types are immiscible, despite the fact that the overall crystal is continuous with regards to the framework.

Discussion

Although there is no sharp structural break between Ma and Me, scapolite should be considered as two binary solid-solution series that meet at Me_{75}. The Me_{76} is therefore an end member and should be considered as an independent mineral species, as was also suggested by Aitken et al. (1984). The $[Na_4 \cdot Cl]^{3+}$ and $[NaCa_3 \cdot CO_3]^{5+}$ clusters occur in series (a) scapolite, and they are generally ordered. $[NaCa_3 \cdot CO_3]^{5+}$ and $[Ca_4 \cdot CO_3]^{6+}$ clusters in series (b) scapolite, and they are disordered. Clusters from the two series probably cannot be mixed homogeneously because of net charge differences, and so they give rise to chemical domains. These domains seem to occur in the $Me_{79.6}$ sample. The fact that there is no sharp structural break between the Ma and Me end members indicates that all the clusters give rise to similar geometrical effects in the structure, although the clusters are chemically diverse.

Several plots illustrating the variation in chemical composition of scapolite show breaks at Me_{75} (Evans et al., 1969). Figure 12 shows the compositional variations of natural scapolites; it is the same as that observed by Evans et al. (1969). [In plotting Fig. 12 (and Fig. 2), we had the choice of making either the percent Me axis or the cluster axis linear, and the latter was chosen. If the percent Me axis is made linear, the inflection point at Me_{75} is still present but appears more subtle.] Our results show that the observed linear compositional variations are the result of substitution between $[Na_4 \cdot Cl]Si_2$ and $[NaCa_3 \cdot CO_3]Al_2$ in series (a) and substitution between $[NaCa_3 \cdot CO_3]Si$ and $[Ca_4 \cdot CO_3]Al$ in series (b), thus giving rise to the inflection at Me_{75}. These two substitution mechanisms do behave independently. The compositional variations in scapolite are, therefore, explained adequately in terms of the two independent substitution mechanisms given above, and they require the occurrence of only three types of clusters. However, we cannot exclude the possibility that other types of clusters may occur at different compositions.

Antiphase domains are observed only in scapolite containing Cl^-, and they arise from the observed ordering of $[Na_4 \cdot Cl]^{3+}$ and $[NaCa_3 \cdot CO_3]^{5+}$ clusters. Although Oterdoom and Wenk (1983) observed APBs with type b reflections and attribute these to Al-Si ordering, it is possible that the small amount of Cl^- in their sample formed sufficient clusters that are ordered, as in the $Me_{79.6}$ scapolite, and these gave rise to the APBs.

The maximum intensity ratio r of type b to type a reflections occurs for the composition $Me_{37.5}$ (Fig. 2) because ordering of clusters is greatest when there are equal numbers of $[Na_4 \cdot Cl]^{3+}$ and $[NaCa_3 \cdot CO_3]^{5+}$ clusters in the structure. The $Me_{79.6}$ sample (Fig. 2) has a small r value, and this can be explained by ordering of $[Na_4 \cdot Cl]^{3+}$ and $[NaCa_3 \cdot CO_3]^{5+}$ clusters in some parts of the crystal, which is reasonable because chemical analyses of this sample by Evans et al. (1969) indicate that it contains some Cl^-. As searches did not reveal type b reflections in Cl-free samples, series (b) samples and the end member Ma belong to space group $I4/m$. Series (a) samples belong to space group $P4$ or $P4/m$.

Conclusions

Scapolite consists of two binary solid-solution series that meet at Me_{75}. Therefore, a mineral having the Me_{75} composition is a valid end member and should be considered as an independent mineral species. The composition varies by the coupled replacement $[Na_4 \cdot Cl]Si_2 \rightleftharpoons [NaCa_3 \cdot CO_3]Al_2$ in series (a) and by the independent coupled replacement $[NaCa_3 \cdot CO_3]Si \rightleftharpoons [Ca_4 \cdot CO_3]Al$ in series (b). HRTEM images indicate that clusters in series (a) are ordered and give rise to APBs, and that clusters in

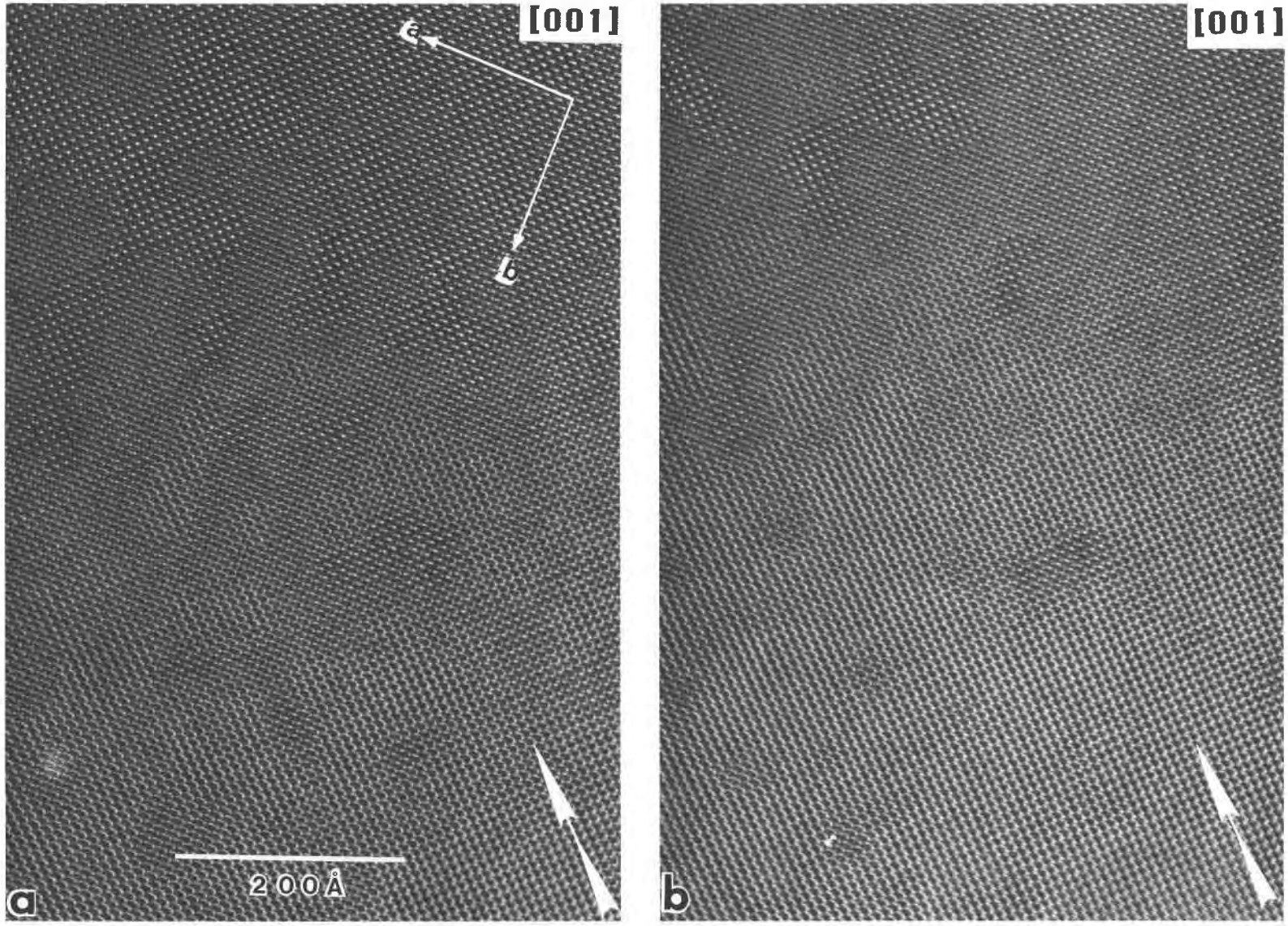

Fig. 11. [001] time-series image from one region of a $Me_{79.6}$ crystal.

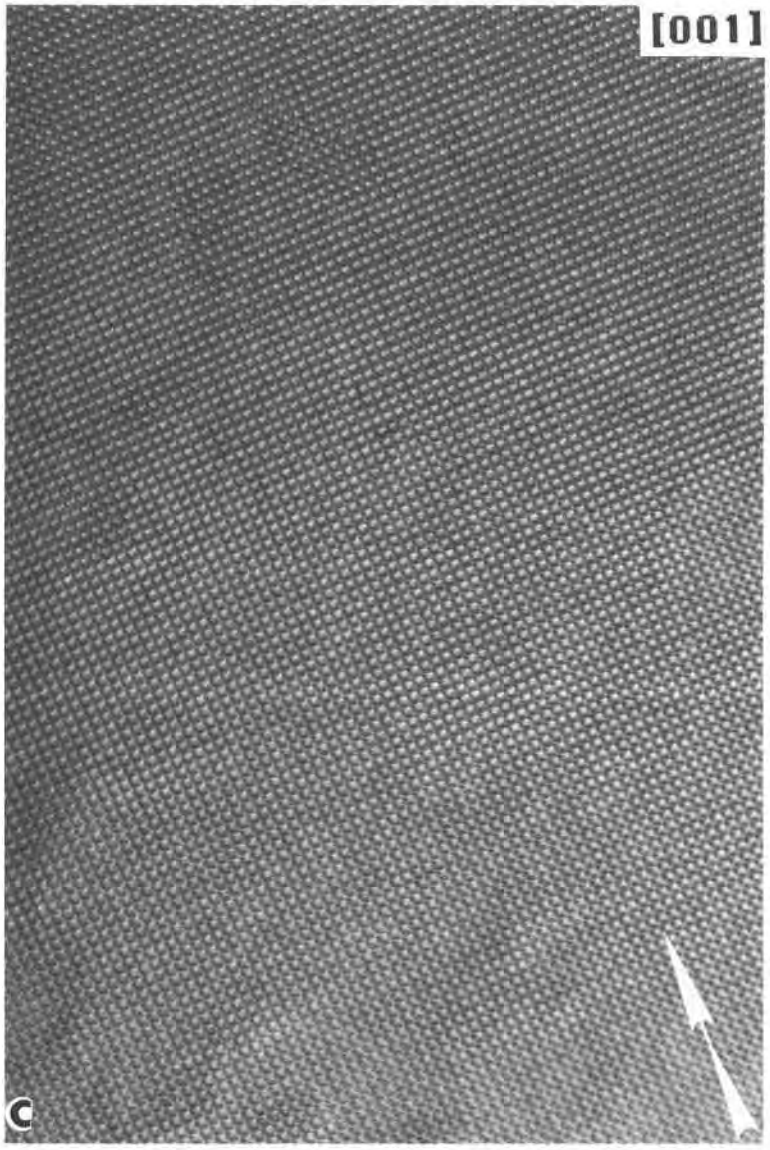

Fig. 11—*Continued.*

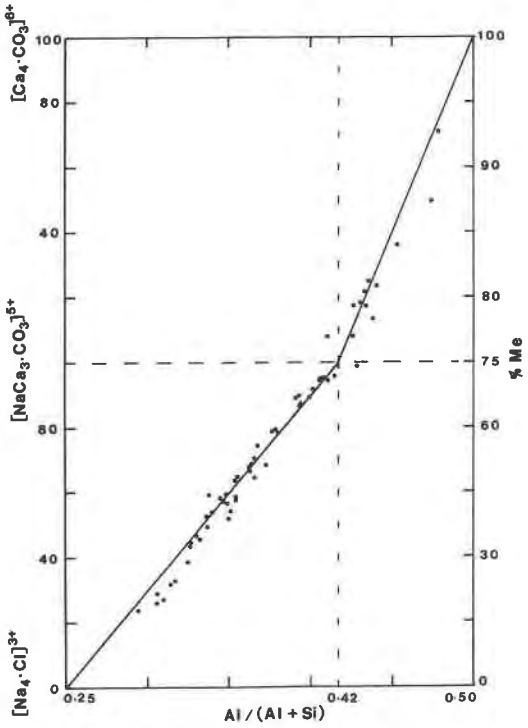

Fig. 12. Al/(Al + Si) vs. % Me, and end-member cluster percentage. The cluster axis and percent Me axis scales are the same as in Figure 2. The solid line represents substitution $[Na_4 \cdot Cl]Si_2 \rightleftharpoons [NaCa_3 \cdot CO_3]Al_2$ in series (a), and $[NaCa_3 \cdot CO_3]Si \rightleftharpoons [Ca_4 \cdot CO_3]Al$ in series (b). Scapolite analyses are from Shaw (1960), Evans et al. (1969), Lin and Burley (1973c), Llambias et al. (1977), Peterson et al. (1979), Graziani and Lucchesi (1982), Aitken (1983), and Oterdoom and Wenk (1983).

series (b) are disordered and so do not give rise to APBs. Series (a) scapolite belongs to space group $P4$ or $P4/m$, and series (b) scapolite belongs to space group $I4/m$, as does the end member Ma. Clusters from the two series cannot be mixed homogeneously because of order arising from net charge difference and give rise to chemical domains, despite the fact that the framework is continuous. Finally, Al–O–Al bonds, which tend to be unfavorable in aluminosilicates, are more numerous in series (b) scapolite; it seems likely that the highly charged $[Ca_4 \cdot CO_3]^{6+}$ clusters stabilize these bonds.

Acknowledgments

The scapolite samples were provided by courtesy of Dennis M. Shaw. We thank John C. Barry and Fred Allen for helpful suggestions and also the two anonymous referees and Jeffrey E. Post, an unofficial referee, for useful comments on this manuscript. This work was supported by NSF Grant EAR-8408169; microscopy was done at the ASU HREM facility, which is supported by NSF and ASU.

References cited

Aitken, B.G. (1983) T-X_{CO_2} stability relations and phase equilibria of a calcic carbonate scapolite. Geochimica et Cosmochimica Acta, 47, 351–362.

Aitken, B.G., Evans, H.T., Jr., and Konnert, J.A. (1984) The crystal structure of a synthetic meionite. Neues Jahrbuch für Mineralogie Abhandlungen, 149, 309–324.

Buseck, P.R., and Iijima, Sumio. (1974) High resolution electron microscopy of silicates. American Mineralogist, 59, 1–21.

Chamberlain, C.P., Docka, J.A., Post, J.E., and Burnham, C.W. (1985) Scapolite: Alkali atom configurations, antiphase domains, and compositional variations. American Mineralogist, 70, 134–140.

Cowley, J.M., and Moodie, A.F. (1957) The scattering of electrons by atoms and crystals. I. A new theoretical approach. Acta Crystallographica, 10, 609–619.

Deer, W.A., Howie, R.A., and Zussman, J. (1963) Rock-forming minerals: 4. Framework silicates. Longmans, London.

Evans, B.W., Shaw, D.M., and Haughton, D.R. (1969) Scapolite stoichiometry. Contributions to Mineralogy and Petrology, 24, 293–305.

Goodman, P., and Moodie, A.F. (1974) Numerical evaluation of N-beam wave functions in electron scattering by the multi-slice method. Acta Crystallographica, A30, 280–290.

Graziani, Giorgio, and Lucchesi, Sergio. (1982) The thermal behaviour of scapolites. American Mineralogist, 67, 1229–1241.

Hassan, I., and Buseck, P.R. (1986) A HRTEM characterization of scapolite solid-solution series (abs.). International Mineralogical Association Abstracts with Program, 120.

Hassan, I., and Grundy, H.D. (1984) The character of the cancrinite-vishnevite solid-solution series. Canadian Mineralogist, 22, 333–340.

——— (1985) The crystal structures of helvite group minerals, $(Mn,Fe,Zn)_8(Be_6Si_6O_{24})S_2$. American Mineralogist, 70, 186–192.

Hassan, I., Peterson, R.C., and Grundy, H.D. (1985) The structure of lazurite, ideally $Na_6Ca_2(Al_6Si_6O_{24})S_2$, a member of the sodalite group. Acta Crystallographica, C41, 827–832.

Klee, W.E. (1974a) Al/Si distribution in tectosilicates: A graph-theoretical approach. Zeitschrift für Kristallographie, 140, 154–162.

——— (1974b) Al/Si distribution in tectosilicates: Scapolites. Zeitschrift für Kristallographie, 140, 163–168.

Levien, Louise, and Papike, J.J. (1976) Scapolite crystal chemistry: Aluminum-silicon distributions, carbonate group disorder, and thermal expansion. American Mineralogist, 61, 864–877.

Lin, S.B. (1975) Crystal chemistry and stoichiometry of the scapolite group. Acta Geologica Taiwanica, 18, 36–48.

Lin, S.B., and Burley, B.J. (1973a) Crystal structure of a sodium and chlorine-rich scapolite. Acta Crystallographica, B29, 1272–1278.

——— (1973b) The crystal structure of meionite. Acta Crystallographica, B29, 2024–2026.

——— (1973c) On the weak reflections violating body-centered symmetry in scapolites. Tschermaks Mineralogische und Petrographische Mitteilungen, 20, 28–44.

——— (1975) The crystal structure of an intermediate scapolite-wernerite. Acta Crystallographica, B31, 1806–1814.

Llambias, E.J., Gordillo, C.E., and Bedlioy, Dora. (1977) Scapolite veins in a quartz monzodiorite stock from Los Molles, Mendoza, Argentina. American Mineralogist, 62, 132–135.

Loewenstein, W. (1954) The distribution of aluminum in the tetrahedra of silicates and aluminates. American Mineralogist, 39, 92–96.

Lovering, J.F., and White, A.J.R. (1964) The significance of primary scapolite in granulitic inclusions from deep-seated pipes. Journal of Petrology, 5, 195–218.

Newton, R.C., and Goldsmith, J.R. (1975) Stability of scapolite meionite ($3CaAl_2Si_2O_8 \cdot CaCO_3$) at high pressures and storage of CO_2 in the deep crust. Contribution to Mineralogy and Petrology, 49, 49–62.

——— (1976) Stability of the end-member scapolites: $3NaAlSi_3O_8 \cdot NaCl$, $3CaAl_2Si_2O_8 \cdot CaCO_3$, $3CaAl_2Si_2O_8 \cdot CaSO_4$. Zeitschrift für Kristallographie, 143, 333–353.

O'Keefe, M.A., and Buseck, P.R. (1979) Computation of high resolution TEM images of minerals. American Crystallographic Association Transactions, 15, 27–44.

O'Keefe, M.A., Buseck, P.R., and Iijima, Sumio. (1978) Computed crystal structure images for high resolution electron microscopy. Nature, 274, 322–324.

Oterdoom, W.H., and Wenk, H.R. (1983) Ordering and composition of scapolite: Field observations and structural interpretations. Contribution to Mineralogy and Petrology, 83, 330–341.

Papike, J.J., and Stephenson, N.C. (1966) The crystal structure of mizzonite, a calcium- and carbonate-rich scapolite. American Mineralogist, 51, 1014–1027.

Papike, J.J., and Zoltai, Tibor. (1965) The crystal structure of a marialite scapolite. American Mineralogist, 50, 641–655.

Peterson, R.C., Donnay, Gabrielle, and LePage, Yvon. (1979) Sulfate disorder in scapolite. Canadian Mineralogist, 17, 53–61.

Phakey, P.P., and Ghose, Subrata. (1972) Scapolite: Observation of antiphase domain structure. Nature Physical Science, 238, 78–80.

Shaw, D.M. (1960) The geochemistry of scapolite. Part I. Previous work and general mineralogy. Journal of Petrology, 1, 218–260.

Sherriff, B.L., Grundy, H.D., and Hartman, J.S. (1986) Al-Si ordering of scapolites from ^{29}Si, and ^{27}Al, MAS NMR (abs.). International Mineralogical Association Abstracts with Program, 229.

Smith, D.J., Saxton, W.O., O'Keefe, M.A., Wood, G.J., and Stobbs, W.M. (1983) The importance of beam alignment and crystal tilt in high resolution electron microscopy. Ultramicroscopy, 11, 263–282.

Stewart, J.M., Ed. (1976) The XRAY system. Technical Report TR-446. University of Maryland, College Park, Maryland, U.S.A.

Strunz, H. (1978) Mineralogische Tabellen. Geest and Porting, Leipzig.

Ulbrich, H.H. (1973a) Crystallographic data and refractive indices in scapolites. American Mineralogist, 58, 81–92.

——— (1973b) Structural refinement of the Monte Somma scapolite, a 93% meionite. Schweizer Mineralogische und Petrographische Mitteilungen, 53, 385–393.

Manuscript received December 5, 1986
Manuscript accepted September 23, 1987